Catalytic enhancement of gold nanocages induced by undercoordination-charge-polarization

Zhang, Xi; Wang, Sanmei; Liu, Yonghui; Li, Lei; Sun, Changqing

2017

Zhang, X., Wang, S., Liu, Y., Li, L., & Sun, C. (2017). Catalytic enhancement of gold nanocages induced by undercoordination-charge-polarization. APL Materials, 5, 053501-.

https://hdl.handle.net/10356/83363

https://doi.org/10.1063/1.4978041

Catalytic enhancement of gold nanocages induced by undercoordination-charge-polarization

Xi Zhang,[1,a] Sanmei Wang,[2] Yonghui Liu,[2] Lei Li,[3] and Changqing Sun[1,a]
[1]*NOVITAS, School of Electric and Electronic Engineering, Nanyang Technological University, 639794 Singapore*
[2]*Key Laboratory of Low-dimensional Materials and Application Technology (MOE) and School of Materials Science and Engineering, Xiangtan University, Xiangtan 411105, China*
[3]*Department of Mechanical and Electrical Engineering, Yangtze Normal University, Chongqing 408100, China*

(Received 30 November 2016; accepted 9 February 2017; published online 16 March 2017)

Principle behind the highest catalytic ability of the least coordinated gold remains a puzzle. With the aid of density functional theory calculations, we show that in 3-coordinated gold cages (i) the Au–Au bond contracts by ~5% in average, (ii) the valance density-of-states shift up to Fermi level when the Au_{55} cluster turns into an Au_{12} cage, and (iii) the activation energy for CO oxidation drops in sequence, Au_{55} cluster (13.6 Kcal/mol), Au_{42} cage (8.0 Kcal/mol), Au_{13}(6.5 Kcal/mol), and Au_{12} cage (5.1 Kcal/mol), with comparing the reaction paths and spin states. The principle clarified here paves the way for the design of gold nanocatalyst. [http://dx.doi.org/10.1063/1.4978041]

Prevailing perception was accepted that gold is a catalytically inactive metal because of the apparent chemical inertness of bulk gold. In fact, the fully occupied Au 5d orbitals can hardly release an electron due to the large first ionization energy. However, in the states of surfaces or nanoparticles, gold can have a large portion of the under-coordinated atoms that induce the ability as a "green," stable, and efficient catalyst in chemical reactions.[1–7]

Under-coordinated sites on the gold nanoparticles can absorb small inorganic molecules such as O_2 and CO, and the presence of these sites is the key to the catalytic properties of supported gold nanoparticles.[8,9] Au nanoparticles were found catalytically active only with a diameter below 3.5 nm.[10–12] A high activity of a gold catalyst occurs when atomic oxygen is bounded in the three-fold coordination sites on gold.[13,14] However, the underlying mechanism of the under-coordination effects remains poorly understood.

In fact, the involvement of under-coordinated atoms either by cluster size reduction or by hollow nanocage formation is indeed fascinating. Under-coordination effects can lead to the contraction of Au–Au bonds at the surface skin,[15–17] deepening of the surface potential well,[18] blue shift of core-level binding energy (Au 4f),[12,19] and red shift and polarization of valance bands.[20,21] Nanoscale gold interacting with photon can excite local surface plasmon,[22] and the resonance peak can be tuned through changing the size of the gold nanocages.[23] Accompanied with the structure evolution of strained icosahedral structures of nanoparticles or nanocages,[24,25] substantial bond contraction occurs on the outermost atomic shell[15,16] that forms the surface "skin."[17] What are the specific functions of under-coordination on the electronic structure and further on the catalytic ability of gold? This paper will address this question.

In 2002, Pyykkö reported that a gold nanocage is stable in the form of icosahedral Au_{12}.[26] Gold nanocages were synthesized[23] and used in nanophotonics,[27] drug delivery,[28] etc. Theoretically, Au_{32}[29] and Au_{42} cages[24] were determined as large stable single-wall cages compared with their

[a]Electronic addresses: zh0005xi@e.ntu.edu.sg and ecqsun@ntu.edu.sg

counterparts in solid nanoparticles, while Au_{50} and Au_{72} do not form stable cages.[29] Compared with the solid nanoparticle catalysis that has been extensively investigated,[8,11,30–32] the catalytic ability of gold nanocages has seldom been studied theoretically.

Although the Langmuir-Hinshelwood mechanism of gold-assisted CO oxidation has been supported by some studies,[31–34] the reaction mechanism is still not entirely clear. In the Langmuir-Hinshelwood mechanism, there are two possible pathways that differ in how O_2 and CO interact with a gold surface. One is an indirect pathway in which O_2 initially undergoes O–O bond cleavage to produce a highly reactive [O] unit.[11] The other is a direct pathway in which the absorbed O_2 directly reacts with CO without undergoing O–O bond cleavage.[30,31,35] Both mechanisms are supported by several groups.

In this paper, we study these two possible mechanisms for the CO oxidation reaction on gold nanomaterials to establish which reaction mechanism is more favorable, using density functional theory (DFT). We mainly focus on the role of the under-coordinated atoms in enhancing the catalytic ability of an Au_{55} solid nanoparticle and a same-diameter nanocage Au_{42} ($Cage_{42}$). Both high-spin and low-spin states are considered in the calculations.

The principle proposed is shown in Eq. (1). The core-level shift of vth energy band E_v of effective coordination number (z) over that of bulk material (B) with respect to energy level of an isolated atom (0) can be expressed as follows:[36]

$$\begin{cases} E_{vi}(0) = \langle v,i|V_{atom}(r)|v,i\rangle & \text{(atomic level)}, \\ E_{vi}(B)-E_{vi}(0) = \left\langle v,i|V_{cry}(r)|v,i\right\rangle + \sum_j f_{ij}(k)\left\langle v,i|V_{cry}(r)|v,j\right\rangle & \\ \quad = \alpha\left(1+\sum_j \frac{f_{ij}(k)\cdot\beta_{ij}}{\alpha}\right)\cong\alpha & \text{(bulk Shift)}, \\ \frac{E_v(z)-E_v(0)}{E_v(\mathrm{B})-E_v(0)} = \frac{\alpha(z)}{\alpha(\mathrm{B})} = \frac{\left\langle v,i|V_{cry}(r)+\delta_{\mathrm{surf}}(z)|v,i\right\rangle}{\left\langle v,i|V_{cry}(r)|v,i\right\rangle} = C_z^{-m} & \text{(core level shift)}, \\ \quad or = \frac{E_v(P)-E_v(0)}{E_v(\mathrm{B})-E_v(0)} & \text{(polarization)}, \end{cases} \tag{1}$$

with

$$\begin{cases} z_1 = 4(1-0.75K^{-1}); z_2 = z_1+2; z_3 = 12 & \text{(effective CN)}, \\ C_z(z) = d(z)/d(B) & \text{(contraction coefficient)}, \\ C_z^{-m} = E_b(z)/E_b(\mathrm{B}) = V_i(z)/V_i(\mathrm{B}) & \text{(bond energy and local potential)}, \end{cases} \tag{2}$$

where $E_v(0)$ is the energy level of an isolated atom. $V_{atom}(r)$ is the intra-atomic potential and $V_{cry}(r)$ crystal potential. $|v, i>$ represents the wave function. $\alpha = <v,i|V_{cry}(r)|v,i>$ is the overlap integral and $\beta_{ij} = <v,i|V_{cry}(r)|v,j>$ the exchange integral whose summation over the first nearest neighbors j contributes to the width of energy band, with a periodic factor $f(k)$ in the form of e^{-ikr} while k being the wave vector. In the localized core-levels, wave functions of core electrons between i and j overlap a little and thus β_{ij} is not comparable to overlap integral of ith atom, α. The core-level shift $E_v(z) - E_v(0)$ is dominated by α. In Eq. (2), m is the bond nature indicator varying with materials. For gold, m has been optimized as 1.[17] z_1, z_2, and z_3 represent effective z of 1st, 2nd, and 3rd layers and the effective z of the first layer of nanoparticle is a function of the reverse particle size K.

According to Eq. (1), as the size of nanoparticle decreases, (i) bonds between under-coordinated atoms become shorter and stronger; (ii) as atoms becomes closer at surface skin, the $V_{cry}(r)$ to the neighbor electron will become deeper; (iii) consequently, α and β_{ij} will be enlarged proportional to the depth of the potential well at equilibrium; (iv) localized core level will shift proportional to α and trapped to deeper energy; (v) valence band polarization (P) happens to the open-shell noble metals: valence band red shifts since nonlocal charges are polarized by densely entrapped core electrons at the under-coordinated sites. Such polarization may turn the ill-coordinated atoms to be a donor-type catalyst, as that happened to Rh adatoms.[37]

Icosahedron was shown to be the most favorable high-symmetric structure for gold nanocages by theoretical[24,29] and experimental[26,38] studies. The surface of an icosahedron gold cluster is composed

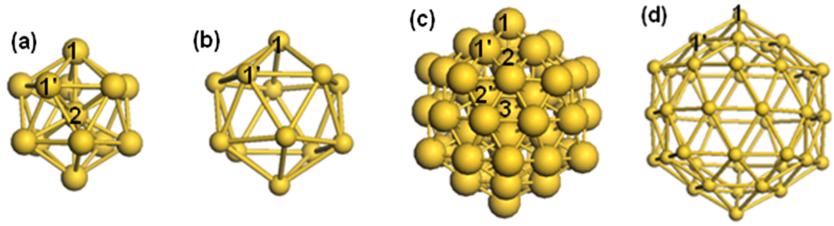

FIG. 1. Structural configuration of (a) Au_{13} and its monolayer (b) $Cage_{12}$, (c) Au_{55} and its monolayer (d) $Cage_{42}$ of ICO structure. Numbers denote the atomic positions.

of twenty distorted triangles and five triangular faces meeting at each vertex, as shown in Figure 1. The Au_{42} cage was discovered as the largest stable gold cages in the icosahedral structure, which contains 20 distorted triangle facets.[24] Figure 1 illustrates the structures of considered gold nanoparticles and nanocages. We choose three different sizes of nanoparticles: icosahedra particles (Au_{13} and Au_{55}) and their monolayer hollow cages ($Cage_{12}$ and $Cage_{42}$), cuboctahedral Au_{147} particle as used for comparison only, as subjects investigated from the angle of size- and layer-dependent energetic properties before and after being used as a catalyst. There are two nonequivalent atomic sites on each facet of $Cage_{42}$. A diatomic molecule can either "dangle" on top of a single gold atom (i.e., 1 or 1' in Figure 1(c)) or "bridge" two gold atoms, i.e., 1-1' or 1'-1' in Figure 1(c). Corner atoms (1) were found to absorb small molecules most easily, with the corresponding binding energy being larger than that for other sites, as reported in previous work.[11,12] We calculated all the possibilities of absorptions and chose a best configuration for each path.

DFT calculations were performed using the DMol[3] code with a double numeric plus polarization basis set to approximate the wave functions. DFT semi-core pseudopotential[39] is chosen as approximations for gold, for dealing with the core potentials including some degrees of relativistic effects. The revised Perdew-Burke-Ernzerhof (RPBE)[40] functional in the framework of the generalized gradient approximation is adopted to describe the exchange-correlation energy, which has been widely used in the calculation of gold nanoparticles. For the DFT calculations, the self-consistency threshold of total energy was set at 10^{-6} hartree. The complete linear/quadratic synchronous transit (LST/QST)[41] technique, which has been used frequently for the investigation of reactions of gold nano-catalysts,[11,30] was used to locate the transition state (TS) in each reaction step. At most five cycles of QST maximum-search calculations were performed, each of which was followed by a conjugate gradient optimization. This was done until the system comes close enough to the saddle point on the potential energy surface. The convergence criteria were set at 10^{-5} hartree for energy, 0.002 hartree/Å for force, and 0.005 Å for displacement. A nudged elastic band (NEB) method[42] search was applied for further searching the energy-minimum state (MS) on the reaction path.

As Eq. (2) expected, bond contraction ($C_z - 1$) indeed occurs between under-coordinated atoms, as listed in Table I. Bonds can be categorized to inter-layer bonds and intra-layer bonds. Single layer cages only have the latter while nanoparticles and double layer cages have both. Diameter D is measured as the distance between two opposite top atom 1. Results of Table I indicate the following:

TABLE I. DFT optimized Au–Au bond length (L), diameters (D), and the contraction coefficient $C_z - 1$ for gold particles and cages. Atom positions are denoted in Fig. 1.

	$Cage_{12}$			Au_{13}			$Cage_{42}$			Au_{55}	
	L (Å)	(%)		L (Å)	(%)		L (Å)	(%)		L (Å)	(%)
1-1′	2.759	−4.3	1-2	2.735	−5.2	1-1′	2.732	−5.2	1-2	2.679	−7.1
			1-1′	2.875	−0.3	1′-1′	2.772	−3.9	1′-2	2.826	−2.0
D	5.25	−4.0	D	5.47		D	10.26	−4.9	1-1′	2.841	−1.5
									2-2′	2.856	−1.0
									2-3	2.716	−5.8
									D	10.79	

(i) The average inter-layer bonds (1-2 and 1′-2) shrink more significantly as size decreases from Au_{147} (2.835 Å), $Cage_{143}$ (2.816 Å), Au_{55} (2.777 Å) to Au_{13} (2.735 Å) compared with Au–Au length 2.88 Å in bulk gold; (ii) the intra-layer bonds (1-1′ and 1′-1′) of cage structures contract more than those of nanoparticles. For example, bond 1-1′ of $Cage_{42}$ (2.732 Å) is much smaller than that of Au_{55} (2.841 Å); (iii) diameters of gold cages also shrink up to 4.9% compared with their solid particle compartments. The Au–Au bond between undercoordinated atoms can be 30% shorter at a few outer shells of gold nanoparticles than that of bulk[15] and the atomic chain.[43] The spontaneous Au–Au bond contraction at the surface has been confirmed thus by both the current DFT calculations[21] and reported experimental measurements.[15] The coordination-resolved Au–Au bond contraction is insensitive to the type of substrate support.[5]

The density of states (DOS) of three sizes of nanoparticles and their cages are shown in Fig. 2(a). The valence band shifts up closing to E_F (set as 0 eV) as the size decreases from Au_{55} to Au_{13}. This trend has also been obtained from cuboctahedral gold particles in previous work.[21] As expected by Eq. (1), the polarization of the hollow cages is more significant than the particles since the atoms in cages are even less-coordinated. As size decreases, the inter-atomic potential shifts deeper accompanied with bond contraction as size decreases. The quantum entrapment has been evidenced by the Au 4f core-level shift amounted at 40% from 2.86 to 4.0 eV with respect to the energy level of an isolated atom at 81.50 eV.[12,18] The valence charges of gold particles are polarized by the densely trapped and tightly trapped core charge due to the deepened potential. Bulk gold is known to be the noblest of all metals: unlike other transition metals of which the 5*d* band locates close to Fermi level (E_F), the Au 5d orbitals were fully occupied deeply under E_F.[44] The polarization of valence charge makes the smaller particles and hollow cages more easy to participate in the chemical reactions.

The calculation results of local density of states (LDOS) of each atomic layer are shown in Fig. 2(b). The major valence charges of the outermost layer (1) are polarized to upper energy while those of the inner layers (2 and 3) remain in the bulk nature. Results indicate that electrons of the undercoordinated surface atoms engage mainly in the catalytic reactions, in accordance with experimental observations.[45] The Au valance bands of the Au monomer and dimer,[45] monatomic chain end,[46] smaller NPs,[21] narrower nanowire,[47] and thinner layers of adatoms[48] have been revealed to be polarized to upper energy compared with that of bulk gold as observed using scanning tunneling spectroscopy.

The energy barrier of CO oxidation without a catalyst is calculated as high as 40.9 kcal/mol. In the Langmuir-Hinshelwood mechanism, there are two possible pathways argued: an indirect pathway in which O_2 initially undergoes O–O bond cleavage[11] and a direct pathway in which the absorbed O_2 directly reacts with CO first.[30,31,35] Hence, in this case, we considered two pathways (**Paths 1** and **2**) for calculation. **Path 1** corresponds to an indirect mechanism that involves initial homolytic cleavage of O_2 on the gold surface and the resultant [O] oxidizes CO. **Path 2** is a direct pathway on which O_2 on the gold surface directly oxidizes CO. The energy profiles for **Paths 1** and **2** are shown in Figures 3(a) and 3(b), respectively. Au_{55} and Au_{13} have unpaired electron. Moreover, O_2 prefer triplet states. Therefore, we considered both high and low spin states for the reactions. The energy

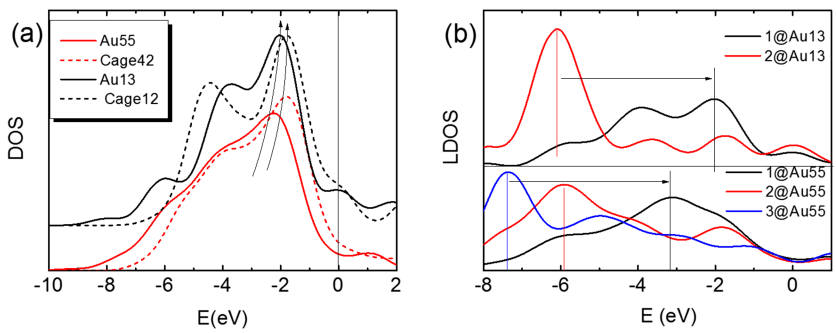

FIG. 2. (a) Comparison of the resultant DOS of the solid nanoparticles (solid lines) and the hollow cages (dashed lines). (b) Atomic layer resolved LDOS of the Au_{13} and Au_{55} structures.

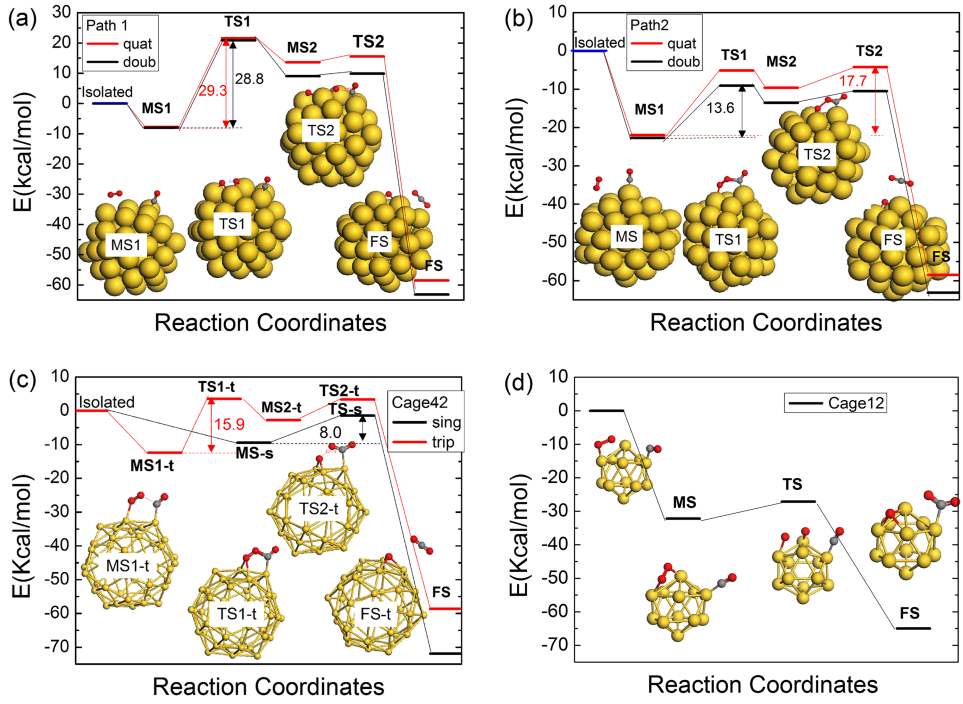

FIG. 3. (a) Energy profile for the reaction of Au_{55} in **Path 1** (indirect path). MS1: absorption of O_2 and CO on gold; TS1: O–O dissociation; TS2: O rotation; and (b) **Path 2** (direct path). TS1: O_2 rotation towards CO; TS2: O–O dissociation by CO. (c) Energy profile of direct path of $Cage_{42}$ in the singlet and triplet spin states. (d) Energy profile of indirect path of $Cage_{12}$.

barrier is calculated by "energy span": the energy difference between highest and lowest energy in the reaction path.[49]

Calculation results of reaction paths for gold nanoparticles and cages are representatively shown in Fig. 3. CO oxidation in the Langmuir-Hinshelwood mechanism prefers the direct reaction path for Au_{55} and Au_{42}, and the indirect reaction path for Au_{13} and Au_{12}, respectively. This is partially due to the less stability of the extremely small cages and nanoparticles. Direct path has more advantages as discussed below. For Au_{55}, as shown in Figs. 3(a) and 3(b), **Path 2** has a lower total energy barrier (13.6 kcal/mol) than **Path 1** (28.8 kcal/mol). In **Path 1,** the barrier is determined by the O–O dissociation on gold, whereas in **Path 2**, the energy barrier is determined by O_2 rotation towards CO (13.6 Kcal/mol) and also O–O dissociation energy (13.5 Kcal/mol). In **Path 2**, O–O dissociation energy is much lowered than **Path 1** with the aid of C attraction. Thus, direct path is more favorable in relatively large nanoparticles and nanocages.

Unexpectedly, although O_2 prefers a spin-triplet state, low spin states are all preferred by nanoparticles and nanocages. As shown in Fig. 3(c), $Cage_{42}$ has a lower energy barrier of 8.0 kcal/mol than triplet state (15.9 kcal/mol) in the reaction than triplet state. The absorption of O_2 and CO on $Cage_{42}$ directly leads to an O_2–CO-interacting **MS** in singlet state, while an energy barrier exists when O_2 approaches to CO in triplet state. $Cage_{42}$ and $Cage_{12}$ structures are stable in the catalytic process. Lower spin states are more favorable since the local O_2 molecular orbitals are mixed with the delocalized 5d orbitals in high-symmetric gold nanoparticles and nanocages.

Mulliken charge analysis shows that for doublet spin state in **Path 2**, Au_{55} donates 0.33 e^- in MS2 and 0.55 e^- in FS, while O_2 accepts 0.52 e^- in MS2 and [O] accepts 0.55 e^- in FS. In singlet spin, $Cage_{42}$ donates 0.44 e^- in MS and 0.57 e^- in FS, while O_2 accepts 0.63 e^- in MS and [O] accepts 0.57 e^- in FS. The charge transfer indicates that the electron donation ability of gold determines the activity of the O_2 in the reaction. Charge polarizations of cages are more significant than those of solid nanoparticles, leading to the better catalysis.

The absorption energy of CO and O_2 to gold is $E_{absorb} = E_{MS} - E_{Initial}$. E_{absorb} of the gold nanostructures are all negative, indicating that the absorption capability of the surface gold atoms is enhanced from the inert bulky gold. The activation energy of the chemical reaction is

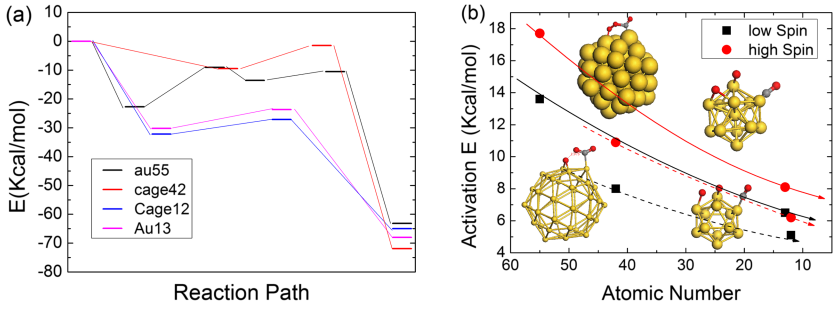

FIG. 4. (a) Comparison of the favorable reaction paths of Au_{55}, $Cage_{42}$, Au_{13}, and $Cage_{12}$. (b) Comparison of the favorable activation energy of Au_{55}, $Cage_{42}$, Au_{13}, and $Cage_{12}$ for both low and high spin states.

$E_{active} = E_{TS} - E_{MS}$. Results in Fig. 4 show that the activation energies of $Cage_{12}$ (5.1 Kcal/mol) and Au_{13} (6.5 Kcal/mol) are much lower than that of $Cage_{42}$ (8 Kcal/mol) and Au_{55} (13.6 Kcal/mol), indicating the better catalytic capability of the even undercoordinated $Cage_{12}$ and Au_{13}. Fig. 4 shows that the absorption ability of CO and O_2 increases from 22.7 Kcal/mol of Au_{55} to 30.2 Kcal/mol of $Cage_{12}$.

Structural fluxionality occurs in hollow cages but it is not significant. For $Cage_{42}$, the local average Au–Au bond length of TS at the absorption sites is 2.788, 3.2% less than the bond length of bulk. For $Cage_{12}$, the local average bond length at the absorption sites of TS is 2.761, 4.1% less than the bond length of bulk. Although the local bond lengths of TS expand compared with the bare cages, they are still less than the bulk length. Combined with the Mulliken charge results, the local bond contraction induced valence charge polarization of gold cage should dominate the catalytic behaviors.

Combined with the results in Figs. 2 and 4, more significant polarization of the valence charges takes the responsibility of the better catalytic properties of smaller-size $Cage_{12}$ and Au_{13}. Besides, the activation energy is reduced from solid particles to hollow cages, since the valence charge polarization of cages is higher due to the even lower coordination. Experimentally observed valence band polarization of Au adatom on TiO_x/Mo(112) surface and their catalytic capability measured by the TOF also verify the polarization-catalysis correlation.[20] The polarization of the valence 4*d* electrons associated with the undercoordinated atoms in the skin of metal nanostructures has been verified as the key for donor-type catalyst like Rh adatoms.[37] The intrinsic activity of perovskite oxide in oxygen evolution reaction also exhibits a strong dependence on the occupancy of the 3*d* band.[50] When the diameter of CTAB-stabilized gold nanoparticle decreases from 56 to 13 nm, the catalytic reaction rate increases from 1.0×10^{-4} s^{-1} to 6.1×10^{-3} s^{-1} for *p*-nitrophenol to *p*-aminophenol reaction.[51] Doping Pt atoms or 4% compression on gold helical nanowires can decrease the O_2 dissociation barriers from 0.85 eV to a more desired 0.6 eV.[52]

In summary, consistency between the theoretical prediction and DFT calculations affirmed the size-dependent surface lattice strain, quantum entrapment, valence charge polarization, and catalytic enhancement of gold particles and cages. The LDOS polarization under E_F witnesses the significance of the ill-coordinated atoms. We particularly emphasized that the under-coordinated surface atoms associated with bond contraction, quantum entrapment, and valence charge polarization dictate the catalytic performance of gold. The polarization of valence band makes the donor-type catalyst more active to lose electrons and engage in the catalytic process. The findings herewith contribute to the understanding of the intrinsic mechanism of catalytic enhancement of undercoordination.

ACKNOWLEDGMENTS

Financial support from MOE Grant Nos. (RG101/14 and RG97/15) Singapore is fully acknowledged.

[1] C. T. Campbell, Science **306**(5694), 234 (2004).
[2] O. Lopez-Acevedo, K. A. Kacprzak, J. Akola, and H. Hakkinen, Nat. Chem. **2**(4), 329 (2010).
[3] A. Wittstock, V. Zielasek, J. Biener, C. M. Friend, and M. Baumer, Science **327**(5963), 319 (2010).

[4] M. S. Chen, D. Kumar, C. W. Yi, and D. W. Goodman, Science **310**(5746), 291 (2005).
[5] J. T. Miller, A. J. Kropf, Y. Zha, J. R. Regalbuto, L. Delannoy, C. Louis, E. Bus, and J. A. van Bokhoven, J. Catal. **240**(2), 222 (2006).
[6] L. Yan, F. Wang, and S. Meng, ACS Nano **10**(5), 5452 (2016).
[7] D. Zijing, G. Shiwu, and M. Sheng, New J. Phys. **17**(1), 013023 (2015).
[8] I. N. Remediakis, N. Lopez, and J. K. Nørskov, Appl. Catal., A **291**(1-2), 13 (2005).
[9] J. A. Rodriguez, S. Ma, P. Liu, J. Hrbek, J. Evans, and M. Pérez, Science **318**(5857), 1757 (2007).
[10] M. Valden, X. Lai, and D. W. Goodman, Science **281**(5383), 1647 (1998).
[11] W. Gao, X. F. Chen, J. C. Li, and Q. Jiang, J. Phys. Chem. C **114**(2), 1148 (2009).
[12] M. Turner, V. B. Golovko, O. P. H. Vaughan, P. Abdulkin, A. Berenguer-Murcia, M. S. Tikhov, B. F. G. Johnson, and R. M. Lambert, Nature **454**(7207), 981 (2008).
[13] T. A. Baker, X. Liu, and C. M. Friend, Phys. Chem. Chem. Phys. **13**(1), 34 (2011).
[14] T. A. Baker, C. M. Friend, and E. Kaxiras, J. Chem. Theory Comput. **6**(1), 279 (2009).
[15] W. J. Huang, R. Sun, J. Tao, L. D. Menard, R. G. Nuzzo, and J. M. Zuo, Nat. Mater. **7**(4), 308 (2008).
[16] W. H. Qi, B. Y. Huang, and M. P. Wang, J. Comput. Theor. Nanosci. **6**(3), 635 (2009).
[17] C. Q. Sun, Prog. Mater. Sci. **54**(2), 179 (2009).
[18] P. Donnadieu, S. Lazar, G. A. Botton, I. Pignot-Paintrand, M. Reynolds, and S. Perez, Appl. Phys. Lett. **94**(26), 263116 (2009).
[19] C. Q. Sun, Phys. Rev. B **69**(4), 045105 (2004).
[20] M. Chen, Y. Cai, Z. Yan, and D. W. Goodman, J. Am. Chem. Soc. **128**(19), 6341 (2006).
[21] X. Zhang, J.-l. Kuo, M. Gu, X. Fan, P. Bai, Q.-G. Song, and C. Q. Sun, Nanoscale **2**(3), 412 (2010).
[22] L. Du, G. Yuan, D. Tang, and X. Yuan, Plasmonics **6**(4), 651 (2011).
[23] S. E. Skrabalak, J. Chen, Y. Sun, X. Lu, L. Au, C. M. Cobley, and Y. Xia, Acc. Chem. Res. **41**(12), 1587 (2008).
[24] Y. Gao and X. C. Zeng, J. Am. Chem. Soc. **127**(11), 3698 (2005).
[25] P. D. Jadzinsky, G. Calero, C. J. Ackerson, D. A. Bushnell, and R. D. Kornberg, Science **318**(5849), 430 (2007).
[26] P. Pyykkö and N. Runeberg, Angew. Chem., Int. Ed. **41**(12), 2174 (2002).
[27] N. Fairbairn, A. Christofidou, A. G. Kanaras, T. Newman, and O. L. Muskens, Phys. Chem. Chem. Phys **15**, 4163 (2012).
[28] Y. Wang, K. C. L. Black, H. Luehmann, W. Li, Y. Zhang, X. Cai, D. Wan, S.-Y. Liu, M. Li, P. Kim, Z.-Y. Li, L. V. Wang, Y. Liu, and Y. Xia, ACS Nano **7**, 2068 (2013).
[29] M. P. Johansson, J. Vaara, and D. Sundholm, J. Phys. Chem. C **112**(49), 19311 (2008).
[30] N. Lopez and J. K. Nørskov, J. Am. Chem. Soc. **124**(38), 11262 (2002).
[31] D. Tang and C. Hu, J. Phys. Chem. Lett. **2**(23), 2972 (2011).
[32] H.-Y. Su, M.-M. Yang, X.-H. Bao, and W.-X. Li, J. Phys. Chem. C **112**(44), 17303 (2008).
[33] C. Shang and Z.-P. Liu, J. Am. Chem. Soc. **133**(25), 9938 (2011).
[34] A. Moghaddasi, M. Zahedi, and P. Watson, J. Phys. Chem. C **116**(8), 5014 (2012).
[35] H.-F. Wang and Z.-P. Liu, J. Am. Chem. Soc. **130**(33), 10996 (2008).
[36] C. Q. Sun, Prog. Solid State Chem. **35**(1), 1 (2007).
[37] C. Q. Sun, Y. Wang, Y. G. Nie, Y. Sun, J. S. Pan, L. K. Pan, and Z. Sun, J. Phys. Chem. C **113**(52), 21889 (2009).
[38] X. Li, B. Kiran, J. Li, H.-J. Zhai, and L.-S. Wang, Angew. Chem., Int. Ed. **41**(24), 4786 (2002).
[39] B. Delley, Phys. Rev. B **66**, 155125 (2002).
[40] B. Hammer, L. B. Hansen, and J. K. Nørskov, Phys. Rev. B **59**(11), 7413 (1999).
[41] T. A. Halgren and W. N. Lipscomb, Chem. Phys. Lett. **49**(2), 225 (1977).
[42] G. Henkelman and H. Jonsson, J. Chem. Phys. **113**(22), 9978 (2000).
[43] C. Q. Sun, H. L. Bai, S. Li, B. K. Tay, C. Li, T. P. Chen, and E. Y. Jiang, J. Phys. Chem. B **108**(7), 2162 (2004).
[44] B. Hammer and J. K. Norskov, Nature **376**(6537), 238 (1995).
[45] J. N. Crain and D. T. Pierce, Science **307**(5710), 703 (2005).
[46] N. Nilius, T. M. Wallis, and W. Ho, Science **297**(5588), 1853 (2002).
[47] K. Schouteden, E. Lijnen, D. A. Muzychenko, A. Ceulemans, L. F. Chibotaru, P. Lievens, and C. V. Haesendonck, Nanotechnology **20**(39), 395401 (2009).
[48] M. Chen and D. W. Goodman, Acc. Chem. Res. **39**(10), 739 (2006).
[49] S. Kozuch and S. Shaik, Acc. Chem. Res. **44**(2), 101 (2010).
[50] J. Suntivich, K. J. May, H. A. Gasteiger, J. B. Goodenough, and Y. Shao-Horn, Science **334**(6061), 1383 (2011).
[51] R. Fenger, E. Fertitta, H. Kirmse, A. F. Thunemann, and K. Rademann, Phys. Chem. Chem. Phys. **14**, 9343 (2012).
[52] J. Yang, B. Li, Q. Zhang, W.-l. Yim, and L. Chen, J. Phys. Chem. C **116**, 11189 (2012).